Theoretical Studies of the O(^3P) + Ethane Reaction†

Diego Troya,‡ Ronald Z. Pascual,§ Donna J. Garton,|| Timothy K. Minton,|| and George C. Schatz*,‡

Chemistry Department, Northwestern University, 2145 Sheridan Road, Evanston, Illinois 60208-3113, Chemistry Department, CAS−University of Southern Mindanao, Kabacan, Cotabato, Philippines 9407, and Department of Chemistry and Biochemistry, Montana State University, Bozeman, Montana 59717

Received: January 6, 2003; In Final Form: March 12, 2003

The O(^3P) + C_2H_6 reaction has been studied at two levels of theory. First, we have carried out high-level *ab initio* calculations of the various asymptotes and stationary points that are relevant to collision energies associated with low Earth orbit (LEO) conditions. CCSD(T)/cc-pVTZ calculations indicate that C−C breakage can occur with energies well below those encountered in LEO and that the barrier for this reaction is the lowest energy other than that for H abstraction to generate OH. Second, we have performed extensive direct dynamics calculations employing the MSINDO semiempirical Hamiltonian and density functional theory (B3LYP/6-31G*) at various collision energies relevant to LEO. OH abstraction is the dominant process at all energies, but other products are also important. Among these, H-atom elimination to give OC_2H_5 + H is the most important, although other products such as H_2O + C_2H_4, OC_2H_4 + 2H, and OCH_3 + CH_3 are also generated at high collision energies. Analysis of product energy distributions reveals the expected trends for H abstraction and H elimination, with the behavior for OCH_3 + CH_3 being closer to that for abstraction. Angular distributions for OH under LEO conditions show forward scattering, whereas those for H elimination and C−C breakage are sideways and backward peaked, respectively. Detailed analysis of the dynamical information will hopefully lead to a better understanding of the microscopic reaction mechanisms of the fundamental processes that contribute to LEO materials erosion.

I. Introduction

Although there have been intense efforts devoted to the simulation of materials erosion in low Earth orbit (LEO),[1,2] the microscopic details whereby materials degrade in this environment are largely unknown. Ground-state atomic oxygen is the dominant species in the 200−700 km LEO altitude range,[3] so often it has been assumed that reactions caused by O(^3P) with hydrocarbon surfaces are similar to those that occur under thermal or low collision energy conditions, leading to the formation of OH radicals.[4] However, LEO conditions are remarkably harsher than those in thermal experiments, and the available collision velocity is roughly 7.4 km/s,[5] corresponding to an O atom with ∼4.5 eV of translational energy striking the ram surface of a spacecraft. At such high energies, new reaction pathways are open, but information about these high energy reaction channels is not available. From an experimental standpoint, only very recently has it become possible to generate a beam of O(^3P) in the laboratory with velocities comparable to those in LEO and with a reasonably narrow spread of velocities.[1,2b,6,7] From a theoretical perspective, O(^3P) reactions with hydrocarbons are difficult to investigate, mainly due to the high dimensionality and large number of open reaction paths. This makes it difficult to use accurate molecular dynamics calculations in combination with high quality electronic structure energies and gradients.

In a parallel study,[8] we carried out dynamics studies of the O(^3P) reaction with the shortest chain alkane, methane, at high collision energies. One of the main conclusions was that even though OH is the dominant product under low collision energies, other products such as H atom elimination take over at higher energies. In this paper we consider a study of the reaction of O(^3P) with the second-shortest-chain saturated hydrocarbon, ethane. This reaction is particularly important because it is the simplest atomic oxygen-saturated hydrocarbon reaction where breakage of a carbon−carbon bond may occur. C−C breakage is supposed to be one of the fundamental processes involved in materials degradation in LEO. As a result, understanding the microscopic mechanism of C−C breakage is of crucial importance to developing a mechanism for the erosion of hydrocarbon polymeric materials. We use gas-phase ethane as a model here, as more accurate theoretical techniques may be utilized for this system than can be used for the polymeric simulations that we will consider later.

An important step in the study of C−C breakage by O(^3P) atoms was presented recently by Massa and co-workers,[9] who performed a quantum chemistry study of the barriers for C−C breakage in the reaction of oxygen atoms with several saturated hydrocarbons including ethane, where the C−C breakage barrier calculated with the complete basis set extrapolation model CBS-QB3[10] was reported to be 1.782 eV. We greatly extend those studies here and consider several other barriers that may be surmounted under LEO conditions and that also contribute to materials erosion. In addition, we carry out molecular dynamics simulations to calculate cross sections and analyze dynamics properties of the various reaction paths, giving a more detailed picture of the fundamental details of materials degradation.

* To whom correspondence should be addressed. E-mail: schatz@chem.northwesternu.edu.

† Part of the special issue "Donald J. Kouri Festschrift".

‡ Northwestern University.

§ CAS−University of Southern Mindanao.

|| Montana State University.

10.1021/jp034028j CCC: $25.00
Published on Web 05/15/2003

TABLE 1: Reaction Energies for the Different $O(^3P) + C_2H_6$ Product Channels[a,b]

	PM3	MSINDO	B3LYP 6-31G*	UMP2 cc-pVTZ	CCSD(T)[c] cc-pVTZ	exp[d]
$OH + C_2H_5$	−1.203(−1.043)	−0.758(−0.589)	0.040(0.234)	0.014(0.196)	0.042(0.223)	−0.08
$H + OC_2H_5$	−0.499(−0.257)	−0.209(−0.007)	0.329(0.563)	0.435(0.654)	0.608(0.827)	0.36
$OCH_3 + CH_3$	−1.254(−1.038)	−0.720(−0.516)	−0.199(0.032)	0.181(0.393)	0.132(0.344)	−0.03
$H_2O + C_2H_4$	−1.965(−1.804)	−1.415(−1.224)	−0.044(0.135)	−0.591(−0.430)	−0.365(−0.204)	
$OC_2H_4 + 2H$	0.297(0.806)	0.644(1.160)	1.082(1.610)	0.612(1.148)	1.163(1.699)	

[a] Energies referred to the $O(^3P) + C_2H_6$ asymptote in eV. [b] Energies in parentheses indicate classical energies, i.e., without zero point energies. [c] CCSD(T)/cc-pVTZ single point calculations using UMP2/cc-pVTZ equilibrium geometries and frequencies. [d] ΔH_{298K} obtained from the experimental heats of formation.[28]

$O(^3P) + C_2H_6$ is also of fundamental interest in combustion chemistry.[11] Thermal rate constants for the lowest barrier reaction, $O(^3P) + C_2H_6 \rightarrow OH + C_2H_5$, have been known for a long time,[12−14] and the recommended expression for the 298−1300 K interval is $(1.8 \times 10^{-31})T^{6.5} \exp(-140/T)$ cm^3 molecule^{-1} s^{-1}.[15] However, there is very little information regarding the dynamics of this reaction. Only recently, McKendrick and co-workers were able to detect the nascent rotational distributions of the OH product coming from the title reaction using $O(^3P)$ atoms generated from NO_2 photolysis at 337, 308, and 248 nm.[16,17] Theoretically, most of the efforts have been devoted to characterizing the lowest barrier stationary points employing quantum chemistry calculations. Jursic employed Moller−Plesset fourth-order calculations with complete basis set extrapolation (MP4/CBSB4) to estimate the reaction barrier, reporting a 0.742 eV value.[18] The reaction energy was evaluated using a higher accuracy model also with complete basis set extrapolation, CBS-Q,[19] and the resulting value (−0.039 eV) is in good agreement with experiments (−0.074 eV). Hase and co-workers[20] carried out CCSD(T)/cc-pVTZ calculations of reaction energy and barrier (0.082 and 0.434 eV, respectively), that were used to reparametrize a PM3 Hamiltonian which was subsequently used in dynamics calculations of $O(^3P)$ atoms with alkanethiolate self-assembled monolayers.

In this work we characterize the reaction energies and barriers of not only the lowest energy reaction but also all of the channels that are open under LEO conditions. In addition, we present a detailed dynamics study employing quasiclassical trajectory calculations, in which the energy gradients are computed on the fly by means of density functional theory (DFT), B3LYP/6-31G*, and using an improved semiempirical Hamiltonian known as MSINDO.

The rest of this paper is structured as follows: section II describes the quantum chemistry calculations, while section III presents the direct dynamics study. Conclusions are presented in section IV.

II. Quantum Chemistry Calculations

As mentioned above, earlier studies of the title reaction have focused only on the lowest energy reaction channel and the C−C breakage saddle point. However, a complete description of all of the product channels open under LEO conditions is still not available. To study these processes, we have used several electronic structure methods including PM3[21] and MSINDO[22−24] semiempirical calculations, B3LYP[25]/6-31G* DFT calculations, and UMP2/cc-pVTZ and CCSD(T)/cc-pVTZ *ab initio* calculations. The PM3 calculations have been carried out using GAMESS,[26] MSINDO calculations have been developed using the standard MSINDO code, and DFT and *ab initio* calculations have been conducted utilizing the Q-Chem[27] package of programs.

Table 1 presents reaction energies for the reactions that may take place under LEO conditions. Only reactions having overall triplet multiplicity have been considered. These reactions include abstraction to give OH, H elimination to give ethoxy, C−C bond breakage to give methoxy plus methyl, double H abstraction to give water plus a triplet diradical C_2H_4, and double H elimination to give acetaldehyde. The table shows that semiempirical calculations always overestimate the exoergicities. The more recently derived MSINDO Hamiltonian systematically improves upon the PM3 results, reducing the error by about 50%, which is a trend very similar to what we saw for $O(^3P) + CH_4$. Considering the $OH + C_2H_5$ products, the more accurate techniques overestimate the experimental reaction energy[28] by a few tenths of an electronvolt. Note that our calculations are done at 0 K, but the measurements correspond to room temperature. However, entropic considerations make the 298 K CCSD(T) reaction energy 0.039 eV more endoergic,[20] deviating even more from experiment. Thus, although CCSD(T) calculations are usually expected to be accurate within chemical accuracy (0.045 eV),[29] the deviations pointed out in Table 1 are substantially larger than this value. We note that we have used the structures optimized at the UMP2/cc-pVTZ level to carry out single point CCSD(T)/cc-pVTZ calculations. To see the effect of the basis set, we have carried out a CCSD(T)/AUG-cc-pVTZ calculation of the $O(^3P) + C_2H_6 \rightarrow OH + C_2H_5$ reaction energy. Inclusion of diffuse functions in the cc-pVTZ basis set[30] provides the desired effect, and the 0 K reaction energy lowers to −0.039 (0.144) eV. The necessity of a very large basis set to accurately describe the lowest barrier reaction energy can also be inferred from Jursic's calculations, where QCISD(T)/6-31+G(d) results gave a very large 0.481 eV 0 K reaction energy, whereas complete basis set extrapolation (CBS-Q)[19] calculations furnished a −0.074 eV value, in good agreement with what we have calculated.

The deviations between theory and experiment for the rest of the reaction energies where measurements are available are analogous to those mentioned above for the lowest reaction energy. The ethoxy + hydrogen asymptote is overestimated by our *ab initio* calculations, B3LYP fortuitously being in excellent agreement with experiments. The products of C−C breakage (methoxy + methyl) are satisfactorily described by DFT and *ab initio* calculations, although we can infer that the basis set is not large enough to provide chemical accuracy. Apart from H abstraction, H elimination, and C−C breakage, there are also several other products possible. Water can also be generated, as has been seen in recent measurements of $O(^3P)$ + squalane,[6] with the C_2H_4 diradical being formed as coproduct. Although $H_2O + C_2H_4$ is the lowest energy product that we report here for the title reaction, we shall see later that the dynamical barrier for this process is large enough to inhibit its formation. Acetaldehyde (CH_3CHO) is also possible upon elimination of two hydrogen atoms. The differences between semiempirical and more accurate theories seem to be reduced for this specific channel.

Table 2 shows the calculated barriers for H abstraction, H elimination, and C−C breakage, and the corresponding saddle point optimized geometries have been plotted in Figure 1. As

TABLE 2: Energy Barriers for the O(^3P) + C_2H_6 → OH + C_2H_5, H + OC_2H_5, and OCH_3 + CH_3 Reactions[a,b]

	PM3	MSINDO	B3LYP 6-31G*	UMP2 cc-pVTZ	CCSD(T)[c] cc-pVTZ
abstraction (TS1)	0.195(0.360)	0.370(0.513)	0.115(0.297)	0.484(0.641)	0.415(0.571)
H elimination (TS2)		1.701(1.879)	1.857(2.037)	2.302(2.441)	2.191(2.330)
H elimination (TS3)	1.122(1.186)	1.671(1.792)	2.110(2.252)	2.533(2.689)	2.457(2.612)
C−C breakage (TS4)		1.645(1.693)	1.692(1.763)	2.278(2.352)	2.062(2.136)
TS5[d]	1.344(1.452)	2.031(2.144)	2.225(2.333)	2.708(2.837)	2.624(2.754)

[a] Energies referred to the O(^3P) + C_2H_6 asymptote in eV. [b] Energies in parentheses indicate classical energies, i.e., without zero point energies. [c] CCSD(T)/cc-pVTZ single point calculations using UMP2/cc-pVTZ optimized geometries and frequencies. [d] See text.

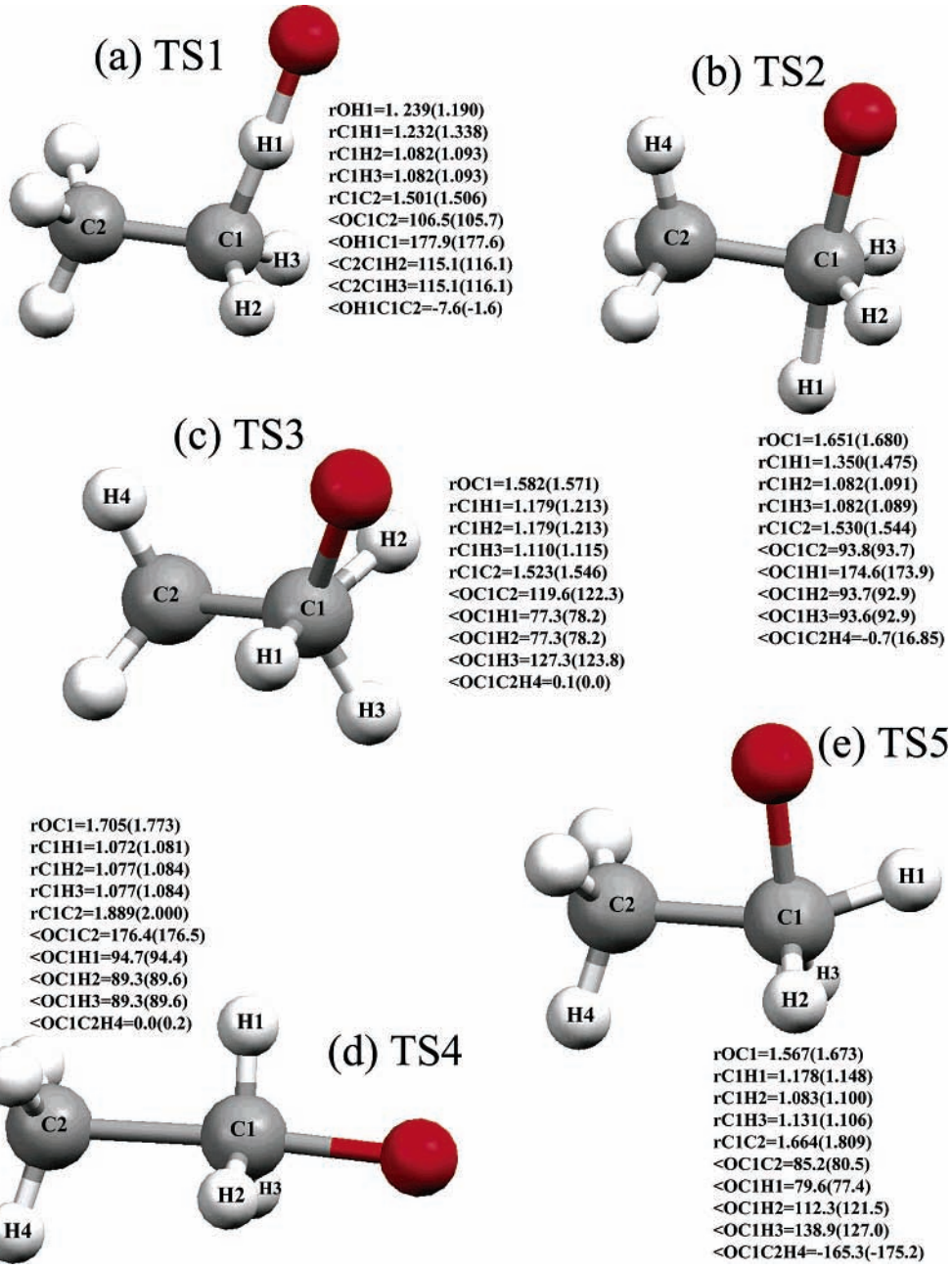

Figure 1. Calculated saddle point structures for O(^3P) + C_2H_6 reactions: (a) saddle point for O(^3P) + C_2H_6 → OH + C_2H_5 denoted as TS1; (b) SN_2-like saddle point for O(^3P) + C_2H_6 → H + OC_2H_5 that we term TS2; (c) near-perpendicular saddle point for O(^3P) + C_2H_6 → H + OC_2H_5 that we term TS3; (d) SN_2-like saddle point for O(^3P) + C_2H_6 → OCH_3 + CH_3 that we term TS4; (e) TS5. See text. Numbers correspond to UMP2/cc-pVTZ calculations, and numbers in parentheses correspond to B3LYP/6-31G* calculations.

is well-known, the lowest energy barrier corresponds to OH formation.[4] The calculations of this barrier are in better agreement with each other than those for the corresponding reaction energies, and noticeably, MSINDO and PM3 show reasonable agreement with more accurate calculations. Figure 1a depicts the DFT and *ab initio* optimized saddle points for abstraction (TS1), showing the nearly collinear O−H−C arrangement typical of H abstraction reactions. To provide an experimental estimate of the barrier height, we have calculated the slope of the Arrhenius plot, based on data from ref 11 in the 298−1000 K range. This gives an activation energy of 0.286 eV, so the barrier height is likely 0.045 eV or so higher. The

most accurate calculations carried out here are somewhat higher still, as also found by Hase and co-workers for the same level of theory.[20] To see if basis set incompleteness is important in this comparison, we have carried out a very demanding (roughly 5 times longer than the corresponding cc-pVTZ calculation) single point calculation of the UMP2 optimized saddle point structure at the CCSD(T)/AUG-cc-pVTZ level, obtaining a barrier of (using the notation of Table 2) 0.318 (0.482) eV. This improves the agreement with the experimental activation energy and reinforces the idea that an enormously large basis set is needed to describe the title reaction within chemical accuracy. It is notable that the MSINDO barrier is in very good agreement with the highest level of *ab initio* theory used in this work, which means that whereas direct dynamics MSINDO calculations of product energy disposal might reflect the wrongly overestimated reaction energy, the cross sections should be accurate.

For H atom elimination to give ethoxy radical, we observe that there are two possible saddle points. This possibility was initially suggested by our earlier calculations on the analogous reaction using methane, where two different saddle points for H atom elimination to give methoxy radicals were identified and shown to contribute to the reactivity under LEO conditions.[8] The lowest energy structure, that we denote TS2 (see Figure 1b), is a S_N2-like saddle point, where the oxygen atom and the exiting hydrogen atom are in a nearly collinear arrangement with the carbon atom that experiences exchange of H for O. The rest of the bonds around the carbon atom are in a quasi-planar arrangement. The reaction barrier for this process is about 2.2 eV, and we note that MSINDO estimates are reasonable compared with higher accuracy calculations. For the second H elimination saddle point, that we denote here as TS3 (see Figure 1c), the incoming oxygen atom and the exiting H atom are no longer in a collinear arrangement but form a rather bent (quasi-perpendicular) angle. The energy of this saddle point is about 0.22 eV above the S_N2-like saddle point in the DFT and *ab initio* calculations, but MSINDO predicts that this structure is 0.17 eV below TS2. For the sake of comparison, we have also calculated the TS3 barrier using standard PM3 calculations, and this shows that MSINDO predictions seem to be much more reliable than PM3 predictions, which for the TS3 saddle point are about 1 eV off compared to more accurate calculations.

As mentioned above, C−C breakage is thought to be one of the fundamental processes leading to materials erosion in LEO. Table 2 also shows the barrier heights calculated in this work for C−C breakage. Drawing inspiration from the two different saddle points possible for H atom elimination, we have looked for the corresponding two stationary points that lead to C−C breakage. Thus, there is a C−C breakage S_N2-like saddle point that we denote here as TS4 (see Figure 1d), in which the exiting group upon O attack to one of the carbon atoms is the whole methyl group bonded to that carbon atom. This is the stationary point also located by Massa and co-workers,[9] whose best estimates based on complete basis set extrapolation[10] and G2[31] models (CBS-QB3 = 1.782 eV; G2 = 1.930 eV) are in good agreement with our CCSD(T)/cc-pVTZ calculations. However, there is a second possibility for C−C breakage that may also take place under LEO conditions. We denote this structure as TS5 (see Figure 1e), and we note that the barrier height for this reaction pathway is 0.45−0.65 eV larger than that for TS4. In Figure 1e it can be seen that the oxygen atom, the carbon atom with which the O−C bond is being formed, and the exiting CH_3 group are in a perpendicular geometry, resembling the TS3 saddle point for H atom elimination. This structure is also reminiscent of an insertion process, which has been traditionally attributed to $O(^1D)$ species.[32,33] Indeed, some of the insertion chemistry observed in LEO erosion has been used as justification for the importance of crossing between the triplet and the singlet potential energy surfaces in the reaction mechanism. Results presented here indicate that $O(^3P)$ insertion in C−C bonds may occur in the absence of triplet−singlet crossing for conditions relevant to LEO.

However, it should be noted that TS5 can lead to two different products depending on the electronic structure method used. Intrinsic reaction coordinate (IRC) calculations that start from the optimized saddle point and go toward the products with a 0.03 a.u. step size lead to $CH_3 + OCH_3$ in B3LYP/6-31G* calculations but to $OC_2H_5 + H$ with the rest of the methods noted in Table 2. No other nearby saddle point leading to the other product could be located. However, this apparent difference between B3LYP/6-31G* and the other methods is not important to the reaction dynamics as we find that collisions that pass through the TS5 region lead to both C−C breakage and H elimination irrespective of the electronic structure method.

MSINDO gives a TS4 energy barrier that is in good agreement with B3LYP calculations, although slightly smaller than is predicted by *ab initio* techniques. Comparisons between PM3 and MSINDO methods are indicated in the table for the saddle point in which the oxygen atom approaches nearly perpendicular to the C−C bond (TS5). The energies obtained with both techniques differ much as they do for the rest of calculations, and whereas the MSINDO barrier height is rather close to the B3LYP calculations, and about 0.65 eV smaller than the higher accuracy *ab initio* calculations, PM3 noticeably underestimates all of the values.

Overall, the MSINDO method consistently improves upon the PM3 calculations, showing its more refined algorithm and parametrization. One of the most common procedures used to carry out dynamics calculations using PM3 has been to reparametrize the PM3 Hamiltonian according to the reaction under consideration.[34] This specific reaction parametrization was indeed applied to the $O(^3P) + C_2H_6 \rightarrow OH + C_2H_5$ reaction by Hase and co-workers in their QM/MM studies of $O(^3P)$ reaction with hydrocarbon self-assembled monolayers.[20] They were able to successfully reduce the exothermicity provided by standard PM3 calculations by about 0.9 eV, subsequently improving the agreement with experiments. However, the improvement in the reaction energy bore the expense of a smaller reaction barrier, which diminished from 0.178 to 0.078 eV at 0 K. It is also easy to infer that the PM3 parameters optimized for $O(^3P) + C_2H_6 \rightarrow OH + C_2H_5$ may not be adequate for the rest of the stationary points and channels we are interested in. Thus, we prefer to use the standard MSINDO semiempirical Hamiltonian that has been shown to be consistently better than the standard PM3 one, rather than reparametrizing the PM3 Hamiltonian to improve the reaction energies at the expense of likely diminishing the accuracy of some of the reaction barriers. Of course, reparametrization can also be done for the MSINDO Hamiltonian, but this is out of the scope of this paper.[35]

III. Dynamics

We have carried out dynamics studies of the title reaction by means of the quasiclassical trajectory (QCT) method. The evaluation of the energy gradients has been done on the fly, that is, while the trajectory is evolved. If the oxygen atom has a 5 eV lab kinetic energy, the collision energy in the center of mass of $O + C_2H_6$ is 3.26 eV. Batches of 10 000 MSINDO trajectories have been run at $E_{coll} = 0.65, 1.50, 2.36, 3.26, 3.92,$

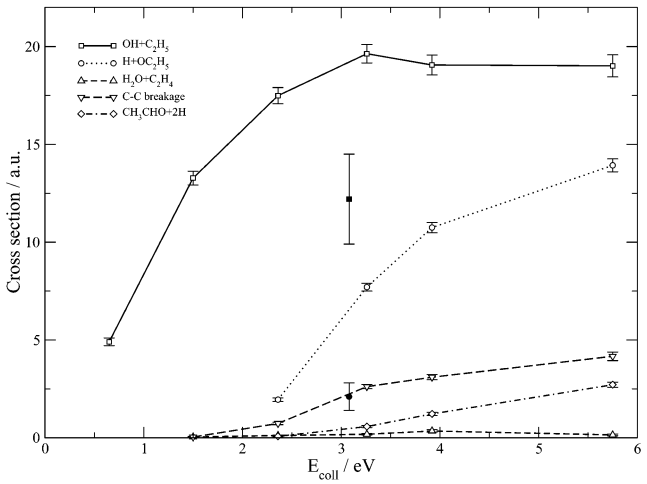

Figure 2. Excitation functions (cross section vs translational energy) for the O(^3P) + C_2H_6 reaction giving OH + C_2H_5, H + OC_2H_5, H_2O + C_2H_4, CH_3CHO + 2H, and C−C breakage. Lines connected with hollow symbols are from MSINDO calculations. Filled symbols are for the respective channels using B3LYP/6-31G* calculations.

and 5.75 eV, while 300 B3LYP/6-31G* trajectories have been calculated at 3.1 eV. The reduced number of B3LYP/6-31G* trajectories is a consequence of the computational expenditure demanded for this kind of calculation in comparison with MSINDO. The cpu time ratio for gradient calculations is MSINDO/B3LYP/6-31G* ≈ 1:3100. The 3 orders of magnitude difference in computation time is further increased when the distance between the oxygen atom and the ethane center of mass or between the product centers of mass is large, because SCF convergence of the B3LYP wave function is more complicated. This has forced us to reduce the initial and final distances of the B3LYP trajectories from 12 au in the MSINDO calculations to about 8 au in B3LYP calculations. The integration time step used in the calculations is also biased for this reason. In the B3LYP calculations, the computational bottleneck is in achieving SCF convergence of the wave function. Therefore, a good initial guess of the orbitals diminishes the overall computation time. In trajectory calculations this can be done by reducing the integration time step, so that the system does not experience large geometry changes from one step to the next and the optimized wave function of a given integration step is close to that of the next point along the trajectory. When doing semiempirical calculations, the SCF convergence/gradients ratio is not so favorable to the gradient calculations and longer integration steps can be used without losing accuracy. Therefore, we have used a 5 au integration step for the B3LYP/6-31G* calculations and 10 au in the MSINDO calculations.

We have utilized the leapfrog algorithm in the DRC subroutine of GAMESS[36] to solve the equations of motion involving B3LYP/6-31G* gradients, whereas we have interfaced MSINDO with a standard fifth-order predictor sixth-order corrector integrator that we have extensively used in our group.[37,38] Maximum sampled impact parameters have been set to 7.5 au for all of the energies but E_{coll} = 0.65 eV, where we set it to 6.5 au. The reactive impact parameter was never larger than 6 au. Ethane initial conditions have been randomly sampled from zero point energy motion.

III.A. Cross Sections. Calculated excitation functions (cross sections vs collision energy) are plotted in Figure 2. The figure shows that the process with the largest cross section throughout the whole interval of translational energies computed is abstraction to give OH, the lowest barrier process. Even under LEO conditions, the OH cross section is larger than the sum of the other possible processes, and only at very high collision energies does the sum of processes other than H abstraction have a larger cross section. This is in contrast to what we learned from analogous calculations on O(^3P) + CH_4,[8] where the H elimination cross section was dominant over abstraction at high energies. The H abstraction cross section increases monotonically up to E_{coll} = 3.26 eV and then the rate of increase slows at larger collision energies. The threshold for H atom elimination to give H + OC_2H_5 is placed at about 2 eV. This is in agreement with the classical barrier (i.e. not including zero point energies) obtained from MSINDO (∼1.8 eV, see Table 2) and even in better agreement with the energy of the adiabatic maximum (1.97 eV). The H elimination cross section increases for the whole range of collision energies considered. Comparison between MSINDO and B3LYP/6-31G* calculations suggests overestimation of the reactivity by the semiempirical technique. The MSINDO/B3LYP ratio for the abstraction cross section is about 1.5, while that for H elimination is about 2; these deviations are consistent with those found in O(^3P) + CH_4.[8] Apart from the different accuracy of the electronic structure methods, an additional source for the discrepancy may be in the small number of total trajectories calculated with the DFT gradients. Indeed, only 25 reactive trajectories for abstraction and 9 reactive trajectories for H elimination were obtained. Hence, the one standard deviation error bars that we display for the B3LYP results are large, and two standard deviations would eliminate much of the difference between B3LYP and MSINDO.

Figure 2 also shows the MSINDO cross sections for C−C breakage, water formation (H_2O + C_2H_4), and acetaldehyde formation (CH_3CHO + 2H). We have observed all of these minority channels in our B3LYP/6-31G* calculations, but only for one individual trajectory in each case, and thus we omit B3LYP cross sections in the graph. Of these minority channels, C−C breakage is the most important, although the cross sections under LEO conditions are not as large as that for H elimination. C−C breakage includes several possible products (OCH_3 + CH_3, CH_2O + CH_3 + H, and CH_3OCH_2 + H), of which methoxy + methyl is the most important under LEO conditions. It is notable that although the lowest energy barriers for C−C breakage and H elimination are within 0.45 eV for both the MSINDO and more accurate *ab initio* calculations, H elimination is dynamically more favored than C−C breakage. This can be understood on the basis of statistical considerations, since when an oxygen atom directly adds to a carbon atom in ethane, there are three hydrogen atoms that can be eliminated but only one CH_3 group that can exit to produce C−C breakage. The H elimination/C−C breakage cross section ratio is 2.7, 3.0, 3.5, and 3.3 for E_{coll} = 2.36, 3.26, 3.92, and 5.75 eV, respectively, which is very close to the value 3.0 that would be expected from statistical considerations.

Acetaldehyde is the fourth most favored product, with a steady increase in cross section throughout the collision energy interval explored. Cross sections for H_2O formation are the smallest and do not seem to increase markedly with collision energy. This is in agreement with recent crossed molecular beams experiments carried out for O(^3P) + methane, ethane, and propane reactions, where products coming from H abstraction, H exchange, or C−C breakage were abundantly found but evidence for H_2O formation was harder to obtain.[2b] It is also noteworthy that the two hydrogen atoms abstracted in the generation of water almost always come from the same carbon atom of ethane. Only at E_{coll} = 5.75 eV, a collision energy much

larger than the average associated with LEO conditions, have we observed a reactive trajectory in which an oxygen atom abstracts two hydrogen atoms originally bonded to the two different ethane carbon atoms.

III.B. Energy Distributions. We begin our analysis of energy distributions in the products by focusing on the most abundant and lowest energy barrier product, OH + C_2H_5. As mentioned above, the OH rotational distributions were recently measured to be cold for OH($v' = 0$), peaking in the $N' = 1-3$ range depending on the O(^3P) precursor photolysis wavelength.[16] The reagent oxygen atoms generated in these experiments have a quite broad energy distribution, and therefore, the translational energy is not unique, but the average (~0.3 eV for 337 nm photodissociation) is lower than the reaction barrier. Our lowest energy MSINDO calculations have been carried out at $E_{coll} =$ 0.65 eV, and therefore, comparisons cannot be done at a quantitative level. Irrespective of this, MSINDO calculations give much hotter OH($v' = 0$) rotational distributions, peaking at $j' = 15$. This difference between theory and experiments is analogous to what was previously seen for O(^3P) + CH_4. There, the MSINDO potential surface was shown to have a looser dependence on the O−H−C bending angle than in the *ab initio* calculations. Looser saddle point bending angles have been demonstrated[39] to increase rotational excitation in the newly formed diatomic, and this seems to apply likewise here for O(^3P) + $C_2H_6 \rightarrow$ OH + C_2H_5. For the OH vibrational distributions, the experiments showed that OH($v' = 1$) is produced, although the OH($v' = 0$)/OH($v' = 1$) ratio was not reported due to the poor signal-to-noise ratio for OH($v' = 1$). Our MSINDO calculations show a 0.63 ± 0.03:0.33 ± 0.02:0.04 ± 0.01 OH-($v' = 0$)/OH($v' = 1$)/OH(v′ = 2) ratio, which is substantially more excited than what can be inferred from experiment. These OH vibrational distributions for O(^3P) + C_2H_6 are indeed more excited than those calculated for O(^3P) + CH_4 for the same translational energy (0.93 ± 0.05:0.07 ± 0.02:0.0 ± 0.0), a trend that is in agreement with experiments. Although the excess rotational excitation in the calculations seems to be tied to inaccuracies in the MSINDO Hamiltonian, the apparently hotter calculated vibrational distributions are not so straightforwardly connected with the approximations in MSINDO. In our earlier QCT calculations of O(^3P) + CH_4 we saw that the abstraction reaction was not vibrationally adiabatic, so the threshold for reaction is smaller than the barrier due to the coupling between the initial zero point energy put in the methane molecule in our QCT calculations and motion along the reaction path.[8] Reducing the initial energy given to methane to half the zero point value gives trajectories in which OH was always in OH($v' = 0$), in agreement with experiments.[16] Giving half the zero point energy (0.25 quanta in each normal mode) to the reagent C_2H_6 in the present work yields colder product OH vibrational distributions (0.73 ± 0.08:0.27 ± 0.05:0.0 ± 0.0 for 9000 trajectories at E_{coll} = 0.65 eV) than when considering trajectories initiated with the usual zero point energy motion of C_2H_6 (0.5 vibrational quanta in each mode). The results with reduced initial zero point energy in the QCT calculations are, in principle, closer to the experimental measurements. We also should bear in mind that the collision energy of the calculations is larger than that in the experiments. Therefore, it seems that the quasiclassical trajectory procedure, in which reagents are given zero point energy for ground-state calculations, is not the most appropriate way of defining initial conditions for systems in which the molecules involved have a large zero point energy content. This problem has been noted before by Hase[40] and can be traced to excessively rapid intramolecular vibrational redistribution associated with the classical mechanical description of large molecules.

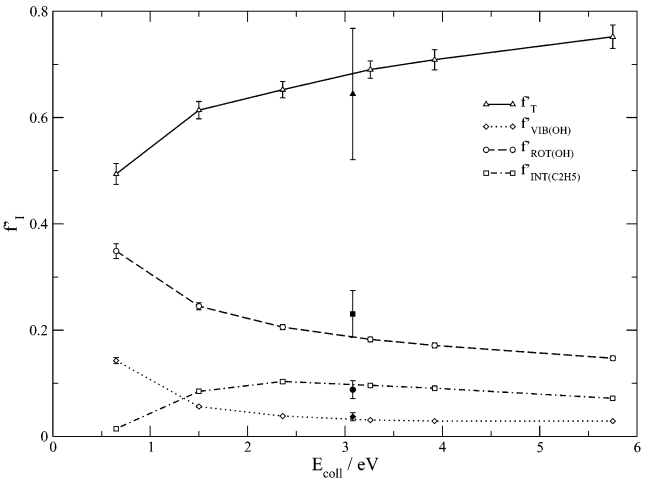

Figure 3. MSINDO and B3LYP/6-31G* average energy fractions in product translation, OH vibration, OH rotation, and C_2H_5 internal energy as a function of collision energy for the O(^3P) + $C_2H_6 \rightarrow$ OH + C_2H_5 reaction. Lines connected with hollow symbols are from MSINDO calculations. Filled symbols are for the respective fractions using B3LYP/6-31G* calculations.

Fortunately, the deficiencies in the electronic structure and dynamics techniques pointed out here are probably less important for the high energies that are of primary interest in this paper. Figure 3 shows the evolution of the average fractions of energy in the product degrees of freedom as a function of initial translational energy for the abstraction reaction. Here we find that energy is released preferentially to translation, much as it was seen in O(^3P) + CH_4,[8] and the average fraction of product translation increases with collision energy. The average fraction of OH vibrational energy decreases with kinetic energy at low energies and remains somewhat constant at higher energies. OH rotation is the second most excited degree of freedom after translation, and the average fractions decrease with increasing collision energy. The ethyl group is noticeably excited, having energy that is substantially above the zero point. This is in contrast with the case of O(^3P) + CH_4, where the energy content of the methyl product was barely above the zero point at all energies studied.[8] Therefore, unlike O(^3P) + CH_4, where the CH_3 fragment is thought to have a near-spectator behavior, in O(^3P) + C_2H_6 substantial energy is released into the ethyl degrees of freedom.

Figure 3 also shows that the B3LYP/6-31G* results are in fairly good agreement with MSINDO results, with average fractions of product translation and OH vibration within statistical uncertainties. However, the B3LYP/6-31G* fraction of OH rotation is smaller than is predicted by MSINDO, likely indicating the higher accuracy of the DFT calculations. As a consequence, the energy release to ethyl is larger in B3LYP calculations. This behavior is identical to what was found in studies of O(^3P) + CH_4.[8]

Now let us consider the energy release to H + OC_2H_5. In this case, we only distinguish between product translation and the internal energy of ethoxy. Figure 4 shows the evolution of the respective average energy fractions as a function of collision energy. Here we see that the average fraction of ethoxy internal energy at the smallest collision energy is below the average fraction of product translation, but the fraction of internal energy becomes larger than that of translation at high energies, and the difference between the two fractions increases with increasing initial translational energy. This is a trend anticipated in

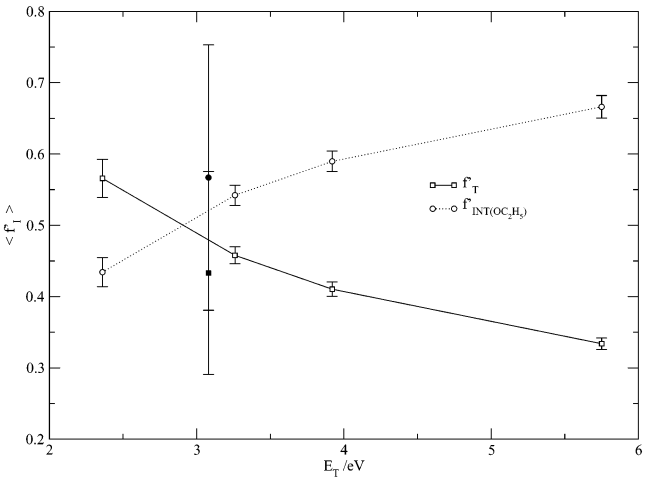

Figure 4. MSINDO and B3LYP/6-31G* average energy fractions in product translation, and OC_2H_5 internal energy as a function of collision energy for the O(^3P) + C_2H_6 → OC_2H_5 + H reaction. Lines connected with hollow symbols are from MSINDO calculations. Filled symbols are for the respective fractions using B3LYP/6-31G* calculations.

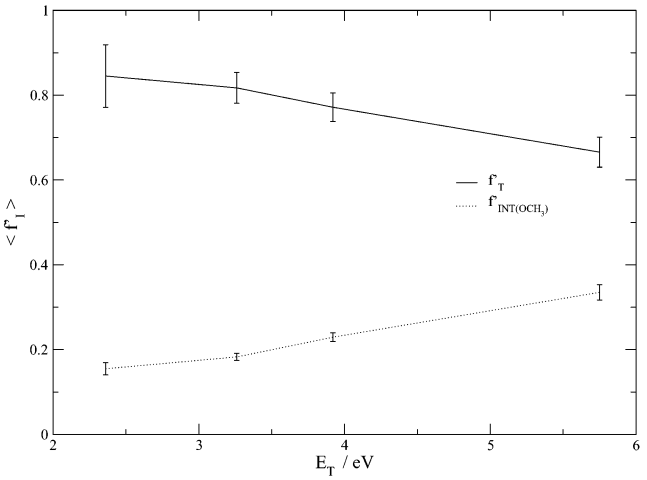

Figure 5. MSINDO average energy fractions in product translation and OCH_3 internal energy as a function of collision energy for the O(^3P) + C_2H_6 → OCH_3 + CH_3 reaction. The average fraction of CH_3 internal energy is zero in all cases. See text.

our studies of O(^3P) + CH_4,[8] and it demonstrates behavior opposite to that of H abstraction, where energy is preferentially released to translation. Although B3LYP/6-31G* and MSINDO calculations agree, we cannot draw solid conclusions about the accuracy of MSINDO in this case, given the large error bars in the B3LYP/6-31G* results.

To finish the analysis of product energy disposal, we have plotted in Figure 5 the average fractions of energy for OCH_3 + CH_3. Here it can be clearly seen that energy is mainly channeled to product translation, which receives about 80% of the available energy at all translational energies. Interestingly, energy release to internal energy of OCH_3 is larger than that to CH_3. Only the OCH_3 result is presented in the figure, as the CH_3 energy is 2−5 kcal/mol below the zero point. Comparing the energy disposal to OCH_3 + CH_3 with that to OH + C_2H_5 and OC_2H_5 + H, it can be seen that the trends obtained for C−C breakage are akin to H abstraction and differ from H atom elimination. Based on well-known results for triatomic reactions following a direct microscopic mechanism,[41−44] we can characterize the dynamics of O(^3P) + C_2H_6 → OH + C_2H_5 using a heavy−light−heavy (HLH) model, whereby most of the energy is released to product translation due to the propensity of the attacking atom to keep its angular momentum (initial orbital angular momentum (**l**) → final orbital angular momentum (**l′**)). O(^3P) + C_2H_6 → OC_2H_5 + H can be pictured as a heavy−heavy−light (HHL) process, where most of the energy appears in the product that contains the incoming heavy atom, since little of the initial orbital angular momentum is converted into product orbital angular momentum. Typically, one would expect that the initial translational energy would end up as the angular momentum of the product molecule that carries the attacking atom (**l** → **j′**); however, we have not decomposed the OC_2H_5 internal energy into rotational and vibrational contributions to verify this. O(^3P) + C_2H_6 → OCH_3 + CH_3 cannot be straightforwardly associated with either of these models, but the analysis of product energy disposal gives evidence that this process is definitely closer to HLH kinematics than to HHL ones.

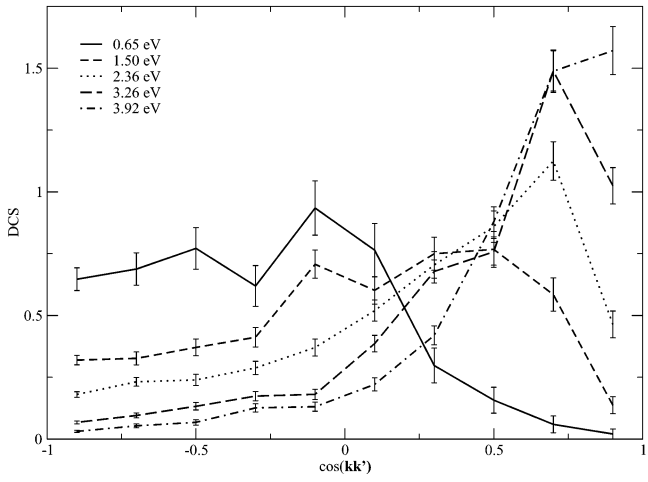

Figure 6. Angular distributions expressed as normalized differential cross sections (DCS, $2\pi/\sigma\ d\sigma/d\Omega'$) for various collision energies for the O(^3P) + C_2H_6 → OH + C_2H_5 reaction.

III.C. Angular Distributions. Figure 6 shows angular distributions for the H abstraction reaction as a function of translational energy expressed as normalized differential cross sections. There is a clear evolution in the scattering from backward to forward with increasing collision energy, as is to be expected for a direct reaction with a near-collinear saddle point.[41,45] This behavior was also pointed out in our previous study of O(^3P) + CH_4. We also note that, in our studies of the influence of the reagent ethane vibrational energy, we see an angular distribution at E_{coll} = 0.65 eV for reaction with half the zero point energy in ethane that is more backward peaked than the one plotted in Figure 6 and which compares better with measurements for homologous reactions with larger hydrocarbons at comparable excess energies above the barrier.[46,47] So, it seems that the quasiclassical enforcement of the initial zero point energy in C_2H_6 has the effect not only of vibrationally exciting the OH product but also of broadening the cone of acceptance, leading to a less backward angular distribution at low collision energies, trends that seem to veer from what is measured in the experiments. B3LYP/6-31G* angular distributions at 3.1 eV are not reported, as the bins generated with 25 reactive trajectories have error bars that are too large to make useful conclusions.

Figure 7 presents the angular distributions for H atom elimination. At the lowest collision energy, there are two peaks that correspond to the two different stationary points described in Figure 1b (TS2) and Figure 1c (TS3) and Table 2. The saddle point TS2 is the S_N2-like structure, and it is responsible for the backward peak at E_{coll} = 2.36 eV (the H atom is scattered in

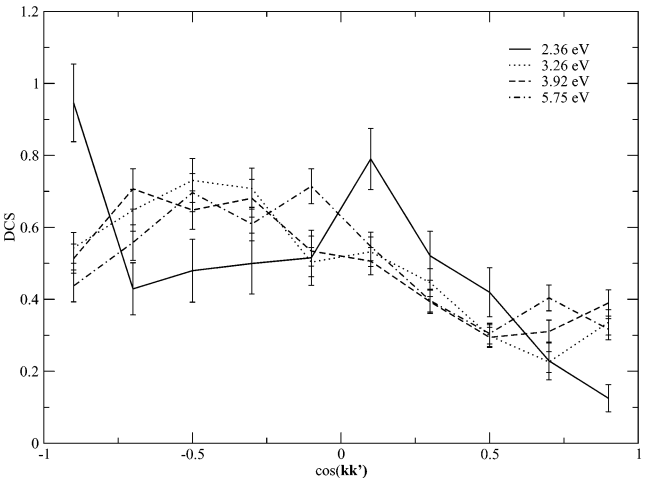

Figure 7. Angular distributions expressed as normalized differential cross sections (DCS, $2\pi/\sigma\ d\sigma/d\Omega'$) for various collision energies for the $O(^3P) + C_2H_6 \rightarrow OC_2H_5 + H$ reaction.

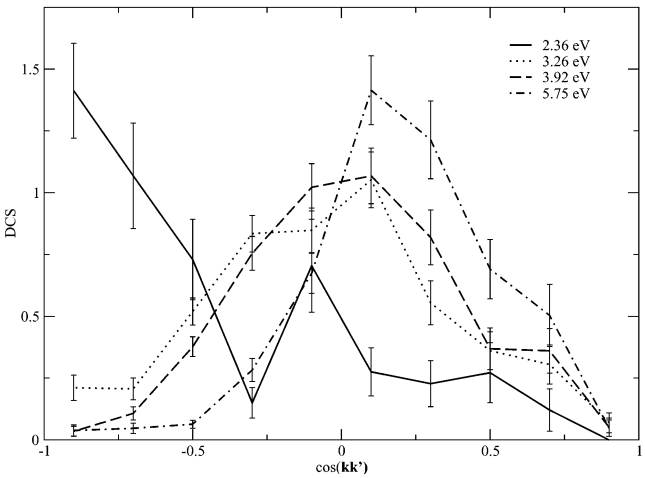

Figure 8. Angular distributions expressed as normalized differential cross sections (DCS, $2\pi/\sigma\ d\sigma/d\Omega'$) for various collision energies for the $O(^3P) + C_2H_6 \rightarrow OCH_3 + CH_3$ reaction.

the same direction as the incoming oxygen atom) due to the collinear arrangement of the saddle point. Trajectories reacting via saddle point TS3 result in a sideways scattering direction due to the bent arrangement of the incoming oxygen atom, the carbon atom being attacked, and the exiting hydrogen atom. These patterns were also seen in the analogous reaction with methane,[8] and similar to the $O(^3P) + CH_4$ reaction, the distinct contributions from the two saddle points fade at larger energies, and although the majority of the flux seems to be confined in the backward hemisphere, the distributions are significantly broader.

Angular distributions for C−C breakage have been depicted in Figure 8. As with H elimination, at the lowest collision energy plotted the two peaks in the angular distribution can be related to the two principal reaction pathways possible for C−C breakage. The backward peak corresponds to the S_N2-like TS4 saddle point, whereas the sideways peak emerges from collisions involving the TS5 region. We do not show in the graph the angular distributions for this process obtained at $E_{coll} = 1.5$ eV due to the low reactivity (cross section $= 0.04 \pm 0.01$ au, with 12 reactive trajectories out of 10 000 calculated), but the results are worth mentioning. 11 of the 12 reactive trajectories fall in the most backward bin, centered at $\cos(\mathbf{kk'}) = -0.9$, and the other goes to the second most backward peak. This is direct evidence obtained in our dynamics calculations that the lowest energy C−C breakage reaction path involves the TS4 saddle point. The geometry of this S_N2-like saddle point leads to backward scattering in which the exiting H atom is scattered in the same direction as the incoming oxygen atom. Trajectories with $E_{coll} = 1.5$ eV have enough energy to surmount the lowest energy barrier (TS4) but not more repulsive bent barriers, thereby resulting in purely backward scattering. As with H elimination, the distinct contributions of the two reaction paths fade with increasing collision energy. Interestingly, the angular distributions seem to shift toward more forward scattering than is the case in the H atom elimination processes. Animation of high energy trajectories reveals that the mechanism associated with C−C breakage is similar to a pure atom abstraction, and the $O(^3P)$ strips off a whole methyl group from the ethane molecule, with very little change in its initial momentum.

IV. Concluding Remarks

We have carried out an extensive study of the $O(^3P) + C_2H_6$ reaction, involving all of the relevant reactive channels that are present under LEO conditions, which include $OH + C_2H_5$, $H + OC_2H_5$, $OCH_3 + CH_3$, $CH_3CHO + 2H$, and $H_2O + C_2H_4$. In the first part of the paper, we present the details of the quantum chemistry of this system, reporting reaction energies and barriers at different levels of electronic structure theory, including PM3, MSINDO, B3LYP/6-31G*, UMP2/cc-pVTZ, and CCSD(T)/cc-pVTZ. Basis sets larger than the standard correlation consistent polarized Dunning triple-ζ basis set are necessary in order to achieve chemical accuracy for the reaction energy and barrier of the minimum energy H abstraction process. Two saddle points for H atom elimination have been identified, one corresponding to a S_N2-like collinear reaction and other to a slightly higher barrier, although also surmountable under LEO conditions, in which the incoming oxygen and the exiting H are arranged nearly perpendicular. Analogous reaction paths are possible for C−C breakage, with energies that are not very different from those for H elimination. MSINDO noticeably improves over PM3, particularly in the reaction barriers, although the predicted reaction energies are noticeably more exoergic than they should be.

Notwithstanding the approximate nature of the MSINDO Hamiltonian, we have conducted the first molecular dynamics study ever reported for the title reaction utilizing the QCT method with MSINDO gradients. B3LYP/6-31G* trajectories have also been computed at a translational energy relevant to the LEO environment. The deficiencies of the MSINDO and QCT methods are evident in the comparison of our calculated product energy disposal with experiments at low kinetic energy, but these errors are likely less important for energies important in LEO, where we focus most of our efforts. Abstraction to give OH is the dominant reactive pathway at all energies, with a threshold below 0.4 eV. The thresholds for the rest of the channels are all very similar (around 2 eV), indicating similar reaction barriers, and H atom elimination to give ethoxy + H is the second most important product. We also report substantial C−C breakage by fast oxygen atom impact, a process crucial to understanding materials degradation in LEO. This result was anticipated in pioneering *ab initio* calculations of the energy barrier,[9] and the present dynamics studies show that C−C breakage and H elimination are both competitive with abstraction at high collision energies.

Our studies of energy release behavior show results that in many cases match the predictions of simple kinematic models. Whereas H abstraction to give OH resembles heavy−light−heavy triatomic reactions, H elimination concurs with heavy−

heavy−light dynamics, and C−C breakage to give methoxy + methyl is closer to abstraction than to elimination. However, it should be noted that these triatomic models are not perfectly suitable for the H abstraction reaction, as there is a substantial fraction of energy released into C_2H_5, which is a product molecule whose bonds are not being formed.

The OH angular distributions are markedly forward under LEO conditions, shifting from backward at low collision energy, as expected for a direct reaction mechanism with a collinear saddle point. In the H elimination angular distributions, we see separate contributions from two saddle points, which fade at high collision energies. The C−C breakage angular distributions are similar to H atom elimination, but we are able to selectively isolate the contribution of the lowest energy reaction path by tuning the translational energy to a value that is sufficient to surmount the lower energy barrier but not higher energy ones.

Comparison with B3LYP/6-31G* calculations, and the knowledge gained in earlier calculations for O(^3P) + CH_4 give credibility to the present MSINDO calculations. Although it is clear that the MSINDO results should not be considered quantitative, the trends reported here should provide a first approximation to the mechanisms involved in materials degradation in LEO.

Acknowledgment. Support for this work comes from AFOSR MURI Grant F49620-01-1-0335 and NSF Grant CHE-0131998. This work was also partially supported by National Computational Science Alliance under Grant No. CHE020027N. G. Lendvay has also contributed to this paper through fruitful discussions. D.J. Garton gratefully acknowledges a fellowship from the Montana Space Grant Consortium.

Note Added after ASAP Posting. This article was posted ASAP on the Web on 5/15/2003. It was inadvertently posted before all the corrections had been incorporated. The correct version was posted on 6/6/2003.

References and Notes

(1) Minton, T. K.; Garton, D. J. Dynamics of Atomic-Oxygen-Induced Polymer Degradation in Low Earth Orbit. In *Advanced Series in Physical Chemistry: Chemical Dynamics in Extreme Environments*; Dressler, R. A., Ed.; World Scientific: Singapore, 2001; p 420.

(2) (a) Murr, L. E.; Kincaid, W. H. *American Scientist* **1983**, *81*, 153; (b) Garton, D. J.; Minton, T. K.; Troya, D.; Pascual, R. Z.; Schatz, G. C. *J. Phys. Chem. A*, in press.

(3) Jursa, A. *U. S. Standard Atmosphere*; U. S. Government Printing Office: Washington, DC, 1976.

(4) Andresen, P.; Luntz, A. C. *J. Chem. Phys.* **1980**, *72*, 5842.

(5) Banks, B. A.; de Groth, K. K.; Rutledge, S. L.; DiFilippo, F. J. *Prediction of In−Space Durability of Protected Polymers Based on Ground Laboratory Thermal Energy Atomic Oxygen*; NASA: Washington, DC, 1996.

(6) Zhang, J.; Garton, D. J.; Minton, T. K. *J. Chem. Phys.* **2002**, *117*, 6239.

(7) Garton, D. J.; Minton, T. K.; Maiti, B.; Troya, D.; Schatz, G. C. *J. Chem. Phys.* **2003**, *118*, 1585.

(8) Troya, D.; Pascual, R. Z.; Schatz, G. C. *J. Phys. Chem. A*, accepted.

(9) Gindulyte, A.; Massa, L.; Banks, B. A.; Rutledge, S. K. *J. Phys. Chem. A* **2000**, *104*, 9976.

(10) Montgomery, J. J. A.; Frisch, M. J.; Ochterski, J. W.; Peterson, G. A. *J. Chem. Phys.* **1999**, *110*, 2822.

(11) Warnatz, J. In *Combustion Chemistry*; Gardiner, J. W. C., Ed.; Springer-Verlag: Berlin, 1984.

(12) Herron, J. T.; Huie, R. E. *J. Phys. Chem.* **1969**, *73*, 3327.

(13) Mahmud, K.; Marshall, P.; Fontijn, A. *J. Chem. Phys.* **1988**, *88*, 2393.

(14) Miyoshi, A.; Tsuchiya, K.; Yamauchi, N.; Matsui, H. *J. Phys. Chem.* **1994**, *98*, 11452.

(15) Cohen, N.; Westberg, K. R. *J. Phys. Chem. Ref. Data* **1991**, *20*, 1211.

(16) Sweeney, G. M.; Watson, A.; McKendrick, K. G. *J. Chem. Phys.* **1997**, *106*, 9172.

(17) Ausfelder, F.; McKendrick, K. G. *Prog. React. Kinet. Mech.* **2000**, *25*, 299.

(18) Jursic, B. S. *J. Mol. Struct.* **2000**, *499*, 91.

(19) Petersson, G. A.; Tensfeldt, T. G.; Montgomery, J. A., Jr. *J. Chem. Phys.* **1991**, *94*, 6091.

(20) Li, G.; Bosio, S. B. M.; Hase, W. L. *J. Mol. Struct.* **2000**, *556*, 43.

(21) Stewart, J. J. P. *J. Comput. Chem.* **1989**, *10*, 209.

(22) Ahlswede, B.; Jug, K. *J. Comput. Chem.* **1999**, *20*, 563.

(23) Jug, K.; Geudtner, G.; Homann, T. *J. Comput. Chem.* **2000**, *21*, 974.

(24) Bredow, T.; Geudtner, G.; Jug, K. *J. Comput. Chem.* **2001**, *22*, 89.

(25) Becke, A. D. *J. Chem. Phys.* **1993**, *98*, 5648. Lee, C.; Yang, W.; Parr, R. G. *Phys. Rev. B* **1988**, *37*, 785.

(26) Schmidt, M. W.; Baldridge, K. K.; Boatz, J. A.; Elbert, S. T.; Gordon, M. S.; Jensen, J. H.; Koseki, S.; Matsunaga, N.; Nguyen, K. A.; Su, S.; Windus, T. L.; Dupuis, M.; Montgomery, J. A. *J. Comput. Chem.* **1993**, *20*, 1347.

(27) Kong, J.; White, C. A.; Krylov, A. I.; Sherrill, C. D.; Adamson, R. D.; Furlani, T. R.; Lee, M. S.; Lee, A. M.; Gwaltney, S. R.; Adams, T. R.; Ochsenfeld, C.; Gilbert, A. T. B.; Kedziora, G. S.; Rassolov, V. A.; Maurice, D. R.; Nair, N.; Shao, Y.; Besley, N. A.; Maslen, P. E.; Dombroski, J. P.; Dachsel, H.; Zhang, W. M.; Korambath, P. P.; Baker, J.; Byrd, E. F. C.; Van Voorhis, T.; Oumi, M.; Hirata, S.; Hsu, C. P.; Ishikawa, N.; Florian, J.; Warshel, A.; Johnson, B. G.; Gill, P. M. W.; Head-Gordon, M.; Pople, J. A. *Q-Chem 2.0*; Q-Chem, Inc.: Export, PA, 2000.

(28) DeMore, W. B.; Sander, S. P.; Golden, D. M.; Hampson, R. F.; Kurylo, M. J.; Howard, C. J.; Ravishankara, A. R.; Kolb, C. E.; Molina, M. J. *Chemical Kinetics and Photochemical Data for Use in Stratospheric Modeling*; Evaluation No. 11, JPL Publ. 94-26; NASA Panel for Data Evaluation, Jet Propulsion Laboratory, California Institute of Technology: Pasadena, 1994.

(29) Knowles, P. J.; Hampel, C.; Werner, H.-J. *J. Chem. Phys.* **1993**, *99*, 5219.

(30) Dunning, T. H., Jr. *J. Chem. Phys.* **1989**, *90*, 1007.

(31) Curtiss, L. A.; Raghavachari, K.; Pople, J. A. *J. Chem. Phys.* **1993**, *98*, 1293.

(32) Luntz, A. C. *J. Chem. Phys.* **1980**, *73*, 1143.

(33) Rudich, Y.; Hurwitz, Y.; Lifson, S.; Naaman, R. *J. Chem. Phys.* **1993**, *98*, 2936.

(34) Gonzalez-Lafont, A.; Truong, T. N.; Truhlar, D. G. *J. Phys. Chem.* **1991**, *95*, 4618.

(35) Bredow, T. Private communication.

(36) Taketsugu, T.; Gordon, M. S. *J. Phys. Chem.* **1995**, *99*, 14597.

(37) Troya, D.; Gonzalez, M.; Schatz, G. C. *J. Chem. Phys.* **2001**, *114*, 8397.

(38) Troya, D.; Lakin, M. J.; Harding, L. B.; Gonzalez, M.; Schatz, G. C. *J. Phys. Chem. B* **2002**, *106*, 8148.

(39) Schatz, G. C.; Amaee, B.; Connor, J. N. L. *J. Chem. Phys.* **1990**, *92*, 4893.

(40) Lu, D.-H.; Hase, W. L. *J. Chem. Phys.* **1989**, *91*, 7490.

(41) Levine, R. D.; Bernstein, L. B. *Molecular Reaction Dynamics and Chemical Reactivity*; Oxford University Press: New York, 1987.

(42) Polanyi, J. C. *Acc. Chem. Res.* **1972**, *5*, 161.

(43) Hijazi, N. H.; Polanyi, J. C. *J. Chem. Phys.* **1975**, *63*, 2249.

(44) Elsum, I. R.; Gordon, R. G. *J. Chem. Phys.* **1982**, *76*, 3009.

(45) Lakin, M. J.; Troya, D.; Lendvay, G.; Gonzalez, M.; Schatz, G. C. *J. Chem. Phys.* **2001**, *115*, 5160.

(46) Liu, X.; Gross, R. L.; Hall, G. E.; Muckerman, J. T.; Suits, A. G. *J. Chem. Phys.* **2001**, *117*, 7947.

(47) Liu, X.; Gross, R. L.; Suits, A. G. *J. Chem. Phys.* **2002**, *116*, 5341.